GPA-RAM: Grasp-Pretraining Augmented Robotic Attention Mamba for Spatial Task Learning

Juyi Sheng*, Yangjun Liu*, Sheng Xu, Senior Member, IEEE, Peiming Li, Zhixin Yang, Senior Member, IEEE, Mengyuan Liu[†], Member, IEEE

Abstract—Task failures in prior fine-grained robotic manipulation methods often stem from suboptimal initial grasping, which is critical for subsequent manipulation and reducing the requirement for complex pose adjustments. To address this, we propose Grasp-Pretraining Augmentation (GPA)—a general multi-modal learning framework that enhances grasp perception without additional grasp pose data collection and labeling. GPA achieves evident enhancement on RLBench multi-task benchmark (from 79.3% to 84.2%) and ALOHA bimanual manipulation tasks (from 86%/16% to 98%/38%). Although GPA enhances finegrained grasping performance by leveraging increased model capacity, it incurs computational latency and hinders real-time deployment. To mitigate this limitation, we propose Robotic Attention Mamba (RAM). This architecture synergizes attention mechanisms with state space models (SSMs), effectively capturing complex spatial features while maintaining superior inference efficiency. Our unified GPA-RAM framework balances model capacity with efficiency and applies to both discrete and continuous action generation. GPA-RAM demonstrates superior performance across four robotic systems with diverse camera configurations in both simulation and the real world. Compared with previous state-of-the-art methods, it improves average success rates by 8.2% over RVT2 (from 79.3% to 87.5%) and 2.6% over ARP+ (from 84.9% to 87.5%) on the RLBench multi-task benchmark and 40% (from 16% to 56%), 12% (from 86% to 98%) on ALOHA bimanual continuous tasks, with inference speed of about 71 FPS. This work provides a framework for developing robotic systems that are simultaneously precise and responsive. The project and code are at https://gpa-ram.github.io/

Index Terms—Robot Learning, Imitation Learning, 3D Manipulation, Multi-modal Perception.

I. INTRODUCTION

R OBOT imitation learning (IL) is a technique where robots acquire skills by observing and mimicking human or other demonstrator actions, making significant progress

*These authors contributed equally to this work.

This work was supported by National Natural Science Foundation of China (No. 62473007), and Shenzhen Innovation in Science and Technology Foundation for The Excellent Youth Scholars (No. RCYX20231211090248064). (Corresponding author: Mengyuan Liu.)

Juyi Sheng, Peiming Li and Mengyuan Liu are with the State Key Laboratory of General Artificial Intelligence, Peking University, Shenzhen Graduate School, Shenzhen, 518055, China (email: logss2024@stu.pku.edu.cn; lipeiming1001@stu.pku.edu.cn; liumengyuan@pku.edu.cn).

Yangjun Liu is with the Shenzhen Institutes of Advanced Technology, Chinese Academy of Sciences, Shenzhen 518055, China, and also with the State Key Laboratory of Internet of Things for Smart City, University of Macau, Macau 999078, China (e-mail: marco.yj.liu@connect.um.edu.mo).

Sheng Xu is with the Shenzhen Institutes of Advanced Technology, Chinese Academy of Sciences, Shenzhen 518055, China (e-mail: sheng.xu@siat.ac.cn).

Zhi-Xin Yang is with the State Key Laboratory of Internet of Things for Smart City, University of Macau, Macau 999078, China (e-mail: zxyang@um.edu.mo).

in robotic manipulation and grasping [1]. This technology accelerates the learning process and reduces reliance on traditional programming by leveraging multi-modal perception capabilities, such as object detection [2] and recognition [3], to accurately parse complex environments. Furthermore, the integration of Vision-Language-Action (VLA) [4] [5] models enables robots not only to capture low-level actions but also to understand semantic contexts, bridging the gap between visual observations, linguistic instructions, and decision-making. Recent advances such as Transformers [6] and diffusion models [7] have proven effective in modeling high-dimensional, multi-modal action distributions, enhancing robots' ability to perform complex tasks. In parallel, the development of lowcost data collection systems [8] (e.g., ALOHA [9], UMI [10]) and large-scale datasets (e.g., RLBench [11] is a discrete action generation benchmark based on key frames, ALOHA [9] is a continuous action generation benchmark.) has lowered entry barriers and further accelerated the progress of IL.

However, as network depth increases, prior methods such as PerACT, RVT, RVT2, ARP+ [9], [12]-[17] face challenges stemming from suboptimal initial grasp detection. These limitations become evident in tasks requiring precise interactions, such as stack cups (see the first row of Fig. 1), and peg-inhole (see the second row of Fig. 1). In the stack cups task, grasp failure occurs early; in the peg-in-hole task, despite successful grasping, inaccurate initial poses prevent successful insertion. These examples highlight that high-precision grasping is critical for subsequent manipulation steps, reducing reliance on complex in-hand adjustments. To address this, we propose Grasp-Pretraining Augmentation (GPA), a general framework adaptable to various robot learning architectures such as ACT [9], RVT2 [16]. As an approach to resolve this challenge in end-to-end manipulation, GPA enhances fine-grained grasp perception without additional pose labels, significantly improving task success rates (Tables V and VI).

While the proposed GPA effectively addresses precision by relying on increased model capacity, this approach consequently introduces an additional critical bottleneck: computational latency. Most existing works rely on Transformers for feature fusion. For instance, leading methods such as PerAct [12], RVT [15] RVT2 [16], and ARP⁺ [17] all utilize Transformers for feature integration on the RLBench multi-task benchmark [11]. Nevertheless, Transformers suffer from quadratic complexity growth when processing long sequences [18]. In the context of vision-based robotics, this computational bottleneck hinders the efficient extraction of fine-grained spatial features from high-resolution multimedia inputs (e.g., multi-view RGB-D streams), which are essential

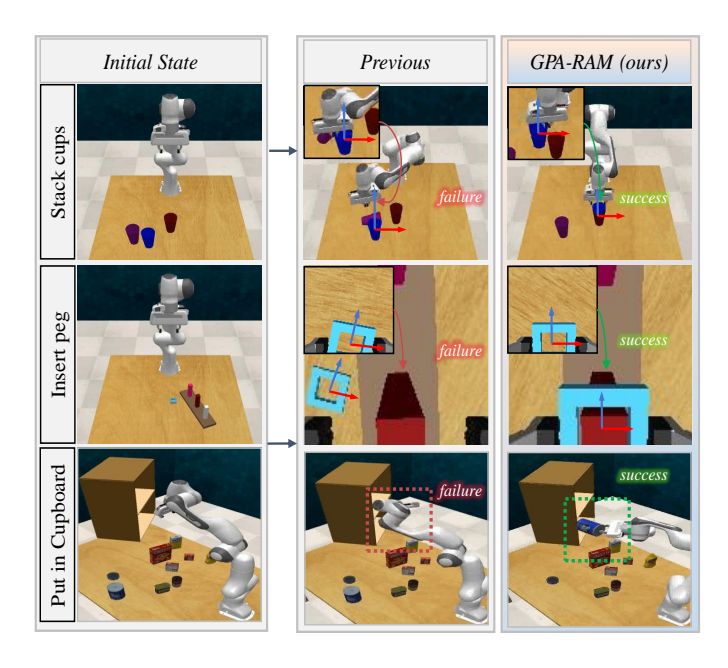


Fig. 1. Previous imitation learning methods struggle with tasks requiring high-precision manipulation and robust spatial perception. This limitation leads to failures such as grasping errors in "Stack the other cups on top of the maroon cup" (top row), imprecise initial grasping and insertion in "Insert the square ring onto the red peg" (middle row), collision caused by poor spatial perception in "Put groceries in the cupboard" (bottom row). In contrast, the proposed Grasp-Pretraining Augmented Robotic Attention Mamba (GPA-RAM) achieves precise manipulation and superior spatial perception.

for precise manipulation. The recent emergence of State Space Models (SSMs) [19] presents a direct solution to this efficiency challenge. Specifically, Mamba, a SSMs architecture, has garnered significant interest as it is capable of linear-time sequence modeling [20]. This design fundamentally avoids the quadratic complexity of Transformers and enables significantly faster inference [20], offering a viable path to maintain high model capacity without sacrificing real-time performance. This motivated us to explore whether Mamba can be integrated with attention mechanisms to enhance both perception and real-time capability. We introduce Robotic Attention Mamba (RAM) — a hybrid architecture designed to efficiently extract spatial features by integrating attention mechanisms, while leveraging Mamba to achieve fast inference speeds. RAM demonstrates strong task performance, maintaining or improving upon previous methods (Table I, II).

By integrating GPA and RAM, this paper proposes a method to mitigate the loss of precise grasping and manipulation perception caused by an over-reliance on global attention, thereby improving the success rate and real-time performance of robot imitation learning across diverse manipulation tasks. The major contributions of this paper are:

- Grasp-Pretraining Augmentation (GPA) is proposed as a general framework adaptable to various robot learning networks for acquiring precise grasping skills critical to downstream manipulation. Grasp perception is enhanced without requiring additional grasp pose labeling.
- We design Robotic Attention Mamba (RAM), a hybrid architecture that integrates linear-time state-space modeling with attention mechanisms, enabling efficient spatial feature capture and real-time action generation in IL.

 The proposed GPA-RAM demonstrates notable empirical performance across diverse tasks in different simulated and real-world robot systems. Specifically, GPA-RAM surpasses previous SOTA methods with an average success rate increase of 8.2% (RVT2), 2.6% (ARP+) on the RLBench discrete multi-task benchmark and 26.0% on the ALOHA bimanual continuous tasks, with higher inference speed.

II. RELATED WORK

A. Vision-Based Robotic Manipulation

IL provides a solution for transferring task-specific expertise from humans to robots, allowing the latter to accomplish manipulations through learning from expert action demonstrations. Classic vision-based learning networks have been developed for robotic grasping. For instance, studies such as [21]–[23] proposed grasp detectors that generate grasp poses and enable task execution. In conventional multi-stage robotic learning methods, [24] proposed a "watch-and-act" pipeline, enabling robots to learn manipulations from visual demonstrations using captioning and affordance-based models. Similarly, [25] introduced a two-stage vision-based approach for efficient submillimeter insertion through reinforcement learning, and [26] proposed a "grasp, see, and place" pipeline for robotic learning. While multi-stage methods improve grasping tasks, they rely heavily on precise execution at each stage, where failure in any sub-task compromises the outcome, increasing complexity and limiting scalability. In contrast, advanced endto-end methods provide a streamlined, lightweight alternative.

The introduction of the ALOHA [9] has gained interest for its ability to learn complex skills, such as cooking, by utilizing visual input. The ALOHA robot employed the ACT algorithm, where an image was taken as input at each step, and the robot predicted future actions based on current visual data. This framework allowed robots to effectively learn and imitate manipulation skills, even in dynamic and complex environments. However, the ACT method was only effective for single-task learning. Building on this, the Diffusion Policy [27] also leveraged visual input to predict future robot actions. Moreover, UMI [10] introduced a low-cost data collection system, significantly reducing the training costs for such models. However, these methods have a key limitation: they are task-specific, requiring separate networks for each manipulation task. This increases computational burdens and leads to exponentially rising costs when addressing various tasks.

To address this challenge, numerous researchers have investigated the use of videos [28]–[32] or combining current images with target task images [33], [34] as inputs to improve model generalization. These approaches enable robots to transfer and share learned skills across tasks, eliminating the need to retrain networks for each task. This not only reduces redundant training but also enhances model efficiency and flexibility in multi-task scenarios.

B. Transformer-Based Robot Learning

The development of Transformer models has evidently enhanced end-to-end methods, particularly in handling multimodal inputs. Relying solely on visual input often falls short in

specifying complex task requirements, prompting researchers to integrate language and vision as complementary inputs. Transformers excel at aligning linguistic and visual features, enabling a more comprehensive understanding of tasks through multimodal fusion. Additionally, contrastive learning further enhances performance by strengthening cross-modal connections, improving task execution accuracy and efficiency. This synergy between visual and linguistic information highlights the potential of Transformers in tackling multimodal tasks.

For instance, PerAct [12] employed a Transformer to encode linguistic goals and RGB-D voxel observations, integrating voxelized 3D action spaces for efficient learning of 6-DOF manipulation tasks. However, the large size of the voxel data slows training. BC-Z [35] addressed the challenge of generalization by enabling robots to adapt to new tasks based on user-provided language or video commands, though its adaptability remains limited. HULC [36] adopted a multimodal Transformer to learn language-conditioned policies from unstructured data. Meanwhile, RVT and RVT2 [15], [16] mitigated the high computational cost of traditional 3D explicit representations (e.g., point clouds) by employing crossview aggregation and virtual re-rendering but failed to focus on fine-grained task manipulation. ARP+ [17] integrated an autoregressive architecture for robotic manipulation. The Σ agent [37] integrated an MVQ-Former to aggregate language information, enhancing robots' understanding and execution of natural language instructions across multi-task scenarios. Combining Transformers with contrastive learning has become a mainstream approach, as seen in RT1 [38], RT2 [39], and FP2AT [40], further improving task performance.

However, existing vision-based robot learning methods primarily focus on the overall process of robot manipulation, failing to achieve precise manipulation and grasping. Transformer methods face challenges like quadratic complexity. In contrast, this paper addresses these limitations by adopting a two-tier skill-learning framework and leveraging the strengths of Mamba. This approach enhances the robot's ability to comprehend task skills and generalize more to novel scenarios.

III. PROPOSED GRASP-PRETRAINING AUGMENTED ROBOTIC ATTENTION MAMBA

We propose the GPA-RAM, as illustrated in Fig. 2. Unlike previous methods, which primarily focus on learning the overall process of manipulation tasks, GPA-RAM is designed to strengthen fine-grained spatial feature extraction and precise manipulation, thereby improving the success rate of task execution. Specifically, we propose two distinct network architectures based on GPA and RAM to handle tasks requiring discrete and continuous actions, respectively.

A. Preliminaries

Problem Statement and Keyframes. In the RLBench [11] task, the robot is supposed to complete M tasks (such as "close jar", "insert onto the square peg", and "open the

drawer") by predicting and execute discrete actions. N expert demonstrations are collected for each task D_k , namely,

$$\mathbf{D}_k = \{ \mathbf{d}_1, \mathbf{d}_2, \mathbf{d}_3 ... \mathbf{d}_N \}, \tag{1}$$

where subscript k denotes the task index. Each demonstration \mathbf{d}_i contains a sequence of language descriptions, observations, actions, and robot states for completing a task, i.e.,

$$\mathbf{d}_i = \left\{ (\mathbf{T}_i, \mathbf{L}_i, \mathbf{O}_1, \mathbf{A}_1, \mathbf{S}_1), \dots, (\mathbf{T}_i, \mathbf{L}_i, \mathbf{O}_n, \mathbf{A}_n, \mathbf{S}_n) \right\},$$
(2)

where $\mathbf{T}_i \in \mathbb{R}^{n_{cams} \times 4}$ is Homogeneous Transformation Matrix, n_{cams} is the camera numbers. \mathbf{L}_i is the description of the current task, such as "open the top drawer". $\mathbf{O}_i \in \mathbb{R}^{n_{cams} \times 7 \times H \times W}$ contains the robot's visual observations, such as RGB images, depth information, or point clouds, and H,W is the image height and width. $\mathbf{A}_i = \left\{\mathbf{a}_{trans} \in \mathbb{R}^3, \mathbf{a}_{rot} \in \mathbb{R}^3, a_{gripper}, a_{collision}\right\}$ represents robot actions, and \mathbf{S}_i denotes the current robotic proprioception. To learn key actions in demonstrations and reduce learning costs, the proposed method designates frames with a speed of zero or changes in the gripper state as key frames following [12], [13], [16], [40]. Thus, the demonstration based on key frames can be denoted as:

$$\mathbf{d}_i = \left\{ (\mathbf{T}_i, \mathbf{L}_i, \mathbf{O}_1, \mathbf{A}_1, \mathbf{S}_1), \dots, (\mathbf{T}_i, \mathbf{L}_i, \mathbf{O}_m, \mathbf{A}_m, \mathbf{S}_m) \right\},$$
(3)

where $m \leq n$. For imitation learning tasks, the vision-language-action model is supposed to predict the next robot keyframe actions from each current observation and robot state, conditioned on the language description \mathbf{L}_i :

$$\mathbf{A}_{t+1} = \mathbf{\Phi}(\mathbf{O}_t, \mathbf{S}_t, \mathbf{L}_i), \tag{4}$$

where t < m represents the time step. Thus, we aim to find an appropriate network Φ that describes the skills from demonstrations, and in other words, Φ is the learned policy for the robot to accomplish M tasks based on expert demonstrations.

Discretization. According to the task description, we can extract pairs of data consisting of $\mathbf{O}_t, \mathbf{S}_t, \mathbf{L}_i$, and action $\mathbf{A}_{t+1} = \left\{\hat{\mathbf{a}}_{trans} \in \mathbb{R}^3, \hat{\mathbf{a}}_{rot} \in \mathbb{R}^3, \hat{a}_{gripper}, \hat{a}_{collision}\right\}$ from the demonstrations. We discretize the $\hat{\mathbf{a}}_{rot}$ angles into 72 categories to represent the full 360 degrees:

$$\overline{\mathbf{a}}_{rot} = [v_1, v_2 \dots v_{72}],\tag{5}$$

where $v_f = 0/1, f \in (0,72]$. For the gripper and collision actions, we binarize the values as follows: $\hat{a}_{gripper} \in \{0,1\}, \quad \hat{a}_{collision} \in \{0,1\}$. Therefore, the ground truth action representation is:

$$\mathbf{A}_{t+1} = [\hat{\mathbf{a}}_{trans}, \overline{\mathbf{a}}_{rot}, \hat{a}_{gripper}, \hat{a}_{collision}]. \tag{6}$$

Mamba. State space models are designed to capture relevant dynamics from high-dimensional systems while filtering out redundant information. The traditional SSMs [20] is represented as:

$$\mathbf{h}_{(t)} = \mathbf{A}\mathbf{h}_{(t)} + \mathbf{B}\mathbf{x}_{(t)},\tag{7}$$

$$\mathbf{y}_{(t)} = \mathbf{C}\mathbf{h}_{(t)},\tag{8}$$

where $\mathbf{A}, \mathbf{B}, \mathbf{C} \in \mathbb{R}^{N \times D}$ are static matrices with fixed dimensions, and index t is the time step. After discretization

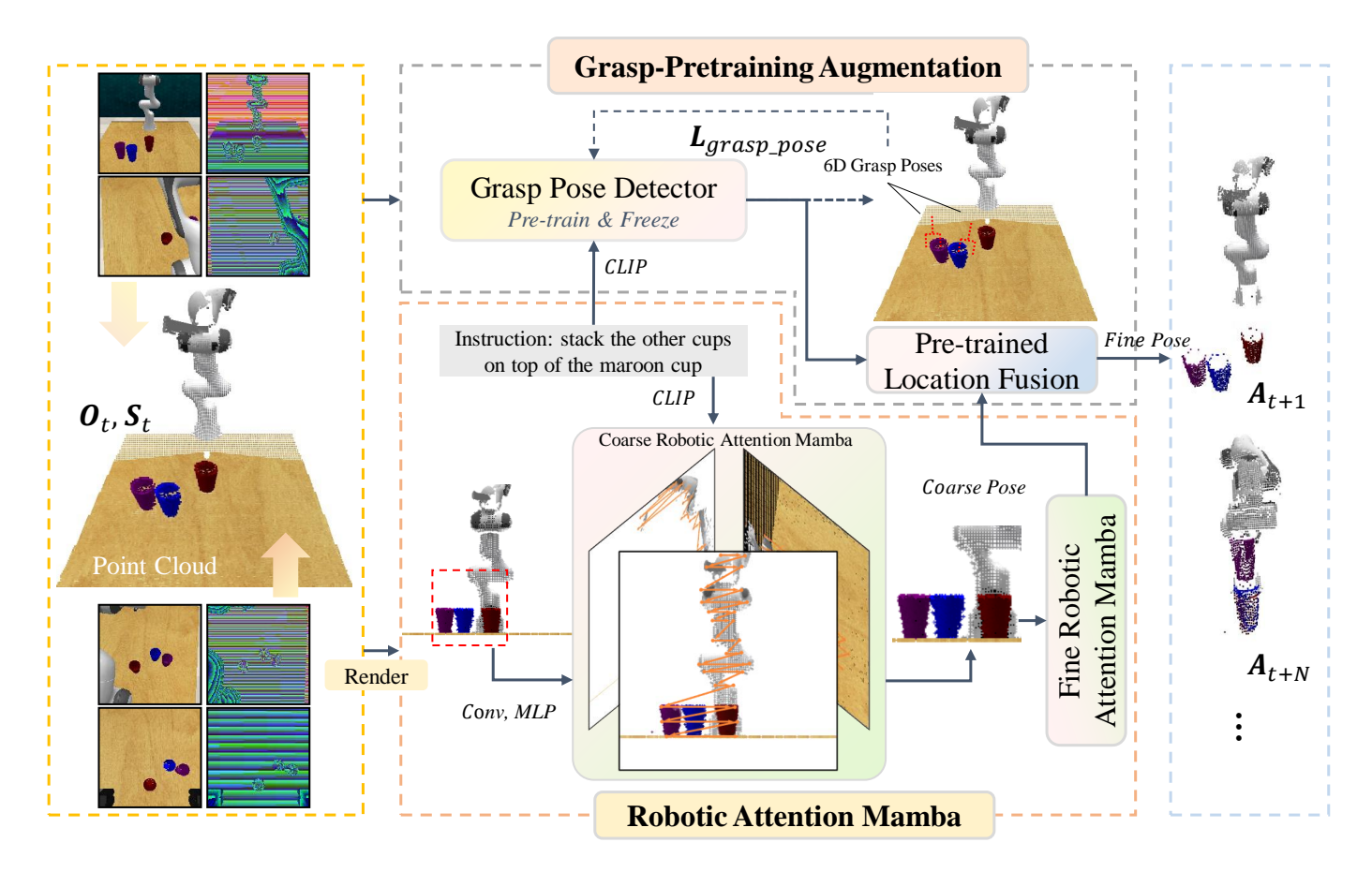


Fig. 2. Overview of the GPA-RAM on RLBench. The GPA-RAM primarily comprises two modules: RAM for spatial features extraction and GPA for grasping skills. It processes point clouds, RGB-D, language instructions, and robot proprioception, extracting spatial semantic features through Coarse and Fine Robotic Attention Mamba in RAM and grasping features via the pre-trained & frozen Grasp Pose Detector in GPA. These features are fused in GPA's Pre-trained Location Fusion to predict the next key action in 3D space.

via zero-order hold, the system can be reformulated using the S4 representation [41]:

$$\overline{\mathbf{A}} = \exp(\Delta \mathbf{A}). \tag{9}$$

$$\overline{\mathbf{B}} = (\Delta \mathbf{A})^{-1} (\exp(\Delta \mathbf{A}) - \mathbf{I}) \cdot \Delta \mathbf{B}, \tag{10}$$

$$\mathbf{h}_t = \overline{\mathbf{A}}\mathbf{h}_{t-1} + \overline{\mathbf{B}}\mathbf{x}_t, \quad \mathbf{y}_t = \mathbf{C}\mathbf{h}_t.$$
 (11)

Here, $\Delta \in \mathbb{R}^D$ represents the input holding step size. However, traditional SSMs are linear time-invariant systems, limiting adaptability as \mathbf{A} , \mathbf{B} , and \mathbf{C} remain static. To overcome this, Mamba extends Δ into $\mathbb{R}^{B \times L \times D}$, enabling each token in a batch to have a unique Δ . This mechanism enables selective forgetting of certain features based on the input, thereby allowing Mamba to dynamically adjust \mathbf{A} , \mathbf{B} , and \mathbf{C} based on input features, enhancing flexibility and adaptability.

B. Overall Network Architecture

The proposed GPA-RAM consists of two key modules. The first, RAM, focuses on efficient spatial feature extraction and achieving high inference efficiency, while the second, Grasp-Pretraining Augmentation, focuses on precise grasping skills and improves initial grasping. Fig. 2 provides an overview of GPA-RAM architecture on the RLBench benchmark for discrete key action prediction, while Fig. 3 presents more details regarding RAM and GPA.

C. Robotic Attention Mamba (RAM)

The first module, RAM, addresses challenges associated with Transformer quadratic complexity and multi-task manipulation, such as improving real-time performance and integrating multi-modal information.

RAM begins with point clouds reconstructed from real RGB-D images O_t , which are rendered into virtual images \mathbf{O}_{tv} from more viewpoints to enhance spatial perception and feature extraction, as shown in Fig. 2. To ensure efficient and precise task learning, RAM employs a coarse-to-fine refinement strategy. In the coarse stage, a Multi-Layer Perceptron (MLP) extracts the robotic proprioception features \mathbf{F}_s . The virtual images \mathbf{O}_{tv} and language descriptions \mathbf{L}_i are fed into Convolutional Layer and Contrastive Language Image Pre-training network (CLIP) [42] to extract virtual image features \mathbf{F}_O and language features \mathbf{F}_L , respectively. The Coarse Robotic Attention Mamba (C-RAM, ϕ_{C-RAM}) takes proprioception features and virtual image features, and task description features as input. After feature extraction through C-RAM, an MLP and Upsample are applied to produce a heatmap \mathbf{Q}_C :

$$\mathbf{F}_{s} = \text{MLP}(\mathbf{S}_{t}), \ \mathbf{F}_{O} = \text{Conv}(\mathbf{O}_{tv}), \ \mathbf{F}_{L} = \text{CLIP}(\mathbf{L}_{i}),$$

$$\mathbf{Q}_{C} = \text{Upsample}\left(\text{MLP}_{1}\left(\phi_{C-RAM}\left(\mathbf{F}_{O}, \mathbf{F}_{s}, \mathbf{F}_{L}\right)\right)\right).$$
(12)

The maximum value in the heatmap corresponds to the coarse

extracted image coordinates (i^*, j^*) . It is represented as:

$$(i^*, j^*) = \operatorname*{max}_{i,j} \mathbf{Q}_C. \tag{13}$$

After performing an upsampling operation at the coarsely extracted coordinates (i^*, j^*) , a new observation \mathbf{Q}' input is obtained. The Coarse process is then repeated using the updated observation \mathbf{O}'_{tv} as input to the Fine Robotic Attention Mamba (F-RAM), yielding the final F-RAM outputs \mathbf{F}_{RAM} :

$$\mathbf{F}_{O}^{'} = \operatorname{Conv}(\mathbf{O}_{tv}^{'}),$$

$$\mathbf{F}_{RAM} = \phi_{F-RAM} \left(\mathbf{F}_{O}^{'}, \mathbf{F}_{s}, \mathbf{F}_{L}\right).$$
(14)

The details of RAM are illustrated in Fig. 3. In each RAM, parallel single-view feature extraction is performed, where image features of each virtual view are processed through a self-attention block to extract independent singleview features with proprioception. These multi-view features are then combined and aligned with task-related language features, extracted using the CLIP [42]. By introducing Mamba following the attention blocks, RAM is supposed to improve spatial perception and real-time performance compared to Transformer-based approaches. Specifically, Mamba effectively models the global context by treating flattened visual patches as continuous sequences. This allows the network to capture long-range spatial dependencies within complex 3D scenes without the heavy computational overhead of full self-attention. Consequently, RAM captures complex semantics with linear complexity, making it particularly effective for robotic manipulation tasks. Afterward, the coarse-to-fine features obtained from Mamba undergo layer normalization, a feedforward network, and residual connections, yielding robust spatial representations for task planning. This design allows the network to progressively refine spatial planning features, balancing global context extraction and fine-grained task prediction for precise robotic manipulation.

In conclusion, the virtual image features, processed through the coarse-to-fine RAM, ensure a strong balance between spatial feature extraction and precise local adjustments, along with critical information attention. This provides a robust and real-time basis for spatial reasoning. Subsequently, it integrates with the following grasping module to further enhance the overall method, enabling both efficient spatial perception and accurate grasping.

D. Grasp-Pretraining Augmentation (GPA)

The second module, GPA, is designed for precise grasping skill enhancement. Given the challenges posed by multitask manipulation based on multi-modal observations, network architectures are designed deep and complex, incorporating multiple layers and modules to handle the intricate requirements of Task and Motion Planning. Some features critical for precise manipulation, such as manipulation affordances of objects and high-resolution grasping cues required for accurate execution after planning, are lost due to the abstraction and generalization of features in deeper layers.

Notably, the whole-task expert demonstrations (such as those utilized by RAM) naturally contain grasp poses of target

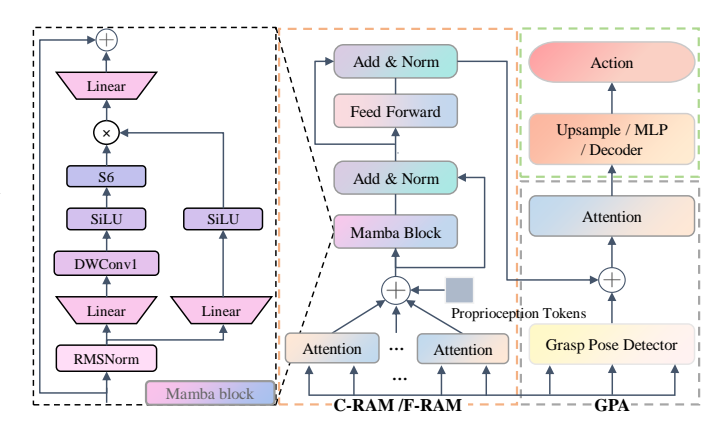


Fig. 3. Network Architecture of Robotic Attention Mamba and Grasp-Pretraining Augmentation. Mamba (Left): Details of the Mamba Block. one-stage RAM (Middle): Visual and robot proprioceptive observations are processed using parallel single-view attention to extract features, which are merged into multi-view and language features for contrastive learning via spatial Mamba blocks. Residual layers, layer normalization, and feedforward layers are applied afterward. GPA (Right): Visual and language features are learned by the grasp pose detector, with spatial attention fusing features from RAM, followed by upsampling and MLP layers for action prediction.

objects alongside spatial manipulation context. Consequently, the proposed GPA employs a novel strategy to explicitly leverage this precise grasping knowledge and mitigate the loss of critical manipulation features, as shown in Fig. 2. GPA, denoted as ϕ_{GPA} , integrates a pre-trained grasp pose detector with a Pre-trained Location Fusion module (PLoFusion), which fuses features from RAM to generate refined task representations \mathbf{F}_{GPA} , defined as follows:

$$\mathbf{F}_{GPA} = \phi_{GPA} \left(\mathbf{O}_t, \mathbf{F}_L, \mathbf{F}_{RAM} \right). \tag{15}$$

The architecture of GPA is detailed in Fig. 3. Prior to task learning, a grasp pose detector is pre-trained using grasp poses extracted from expert demonstrations, enabling it to capture essential grasping features. This information acts as a foundation for improving the model's ability to perceive and manipulate various objects. Subsequently, GPA introduces a fusion mechanism, where features extracted by the pre-trained grasp pose detector are integrated directly into the learning pipeline, as illustrated in Fig. 2 and Fig. 3. Specifically, PLo-Fusion concatenates these pre-trained features with spatially aligned features from the RAM module. The concatenation occurs in the spatial dimension, enabling the model to leverage both detailed grasping insights and broader planning strategies. The merged features are then fused through self-attention, which dynamically balances the focus between global planning and local manipulation, ensuring robustness in complex scenarios. This effectively bridges the gap between high-level and low-level feature representations, ensuring that detailed local information is preserved throughout the task learning process. This approach shortens the knowledge transfer path and maintains critical manipulation skills that are overshadowed by an overemphasis on global planning.

Technically, in the formal training phase, the output head of the pretrained grasp pose detector is removed for feature extraction, and the other parts can be frozen or fine-tuned. By grounding the model in detailed affordance features, GPA lays a strong foundation for high-precision manipulation, com-

plementing the RAM module, which excels in spatial feature perception and inference speed, to deliver improved success rates in diverse challenging robotic tasks.

E. Action Prediction

The features extracted by GPA are fed into different MLPs to predict the gripper state $\mathbf{a}_{gripper}$ and potential collision indicators $\mathbf{a}_{collision}$ and next keyframe rot \mathbf{a}_{rot}' . Meanwhile, these features are upsampled to produce a fine-grained position heatmap, from which the location with the highest activation is selected as the next target position \mathbf{a}_{trans} . The overall process can be formulated as:

$$\mathbf{a}_{rot}^{'}, a_{gripper}^{'}, a_{collision}^{'} = \text{MLPs}\left(\mathbf{F}_{GPA}\right), \\ \mathbf{a}_{trans}^{'} = \underset{\mathbf{a}}{\text{arg max}}\left(\text{Upsample}\left(\text{MLP}\left(\mathbf{F}_{GPA}\right)\right)\right). \tag{16}$$

The prediced actions \mathbf{A}'_{t+1} is written as:

$$\mathbf{A}_{t+1}^{'} = \left[\mathbf{a}_{trans}^{'}, \mathbf{a}_{rot}^{'}, a_{gripper}^{'}, a_{collision}^{'} \right]. \tag{17}$$

The total loss \mathcal{L}_{total} consists of the translation loss \mathcal{L}_{trans} , rotation loss \mathcal{L}_{rot} , gripper loss $\mathcal{L}_{gripper}$, and collision prediction loss $\mathcal{L}_{collision}$:

$$\mathcal{L}_{total} = \lambda_{trans} \mathcal{L}_{trans} + \lambda_{rot} \mathcal{L}_{rot} + \lambda_{gripper} \mathcal{L}_{gripper} + \lambda_{collision} \mathcal{L}_{collision},$$
(18)

where λ_* denotes the weighting coefficient for each term. Each sub-loss is defined as follows. The translation and rotation losses are given by:

$$\mathcal{L}_{trans} = \left\| \mathbf{a}'_{trans} - \hat{\mathbf{a}}_{trans} \right\|_{2}^{2}, \tag{19}$$

$$\mathcal{L}_{rot} = \left\| \mathbf{a}'_{rot} - \overline{\mathbf{a}}_{rot} \right\|_{2}^{2}, \tag{20}$$

where $\|\cdot\|_2$ denotes the ℓ_2 norm, which measures the Euclidean distance and is defined as $\|\mathbf{v}\|_2 = \sqrt{v_1^2 + v_2^2 + \cdots + v_n^2}$ for a vector \mathbf{v} . The gripper and collision prediction losses are formulated using binary cross-entropy:

$$\mathcal{L}_{gripper} = -a'_{gripper} \log(\hat{a}_{gripper}) - (1 - a'_{gripper}) \log(1 - \hat{a}_{gripper}), \tag{21}$$

$$\mathcal{L}_{collision} = -a'_{collision} \log(\hat{a}_{collision}) - (1 - a'_{collision}) \log(1 - \hat{a}_{collision}).$$
(22)

Here, $\hat{\mathbf{a}}_{trans}$, $\overline{\mathbf{a}}_{rot}$, $\hat{a}_{gripper}$, $\hat{a}_{collision}$ are ground-truth. Finally, the network is trained end-to-end by minimizing \mathcal{L}_{total} :

$$\theta^* = \arg\min_{\theta} \mathcal{L}_{total},\tag{23}$$

where θ represents the parameters of the entire framework.

F. Adapt to Continuous Tasks

Different from RLBench, the ALOHA bimanual benchmark requires continuous action prediction at 50Hz. Compared with RLBench, it does not involve language descriptions or the processing of keyframes. Therefore, each demonstration in continuous tasks is represented as:

$$\mathbf{d}_i = \{ (\mathbf{O}_1, \mathbf{A}_1, \mathbf{S}_1), \dots, (\mathbf{O}_n, \mathbf{A}_n, \mathbf{S}_n) \}.$$
 (24)

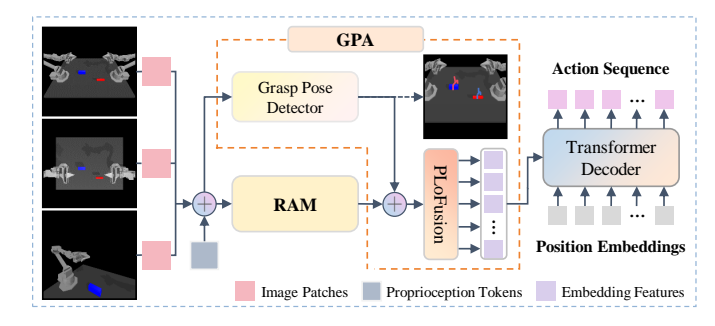


Fig. 4. Adapt GPA and One-Stage RAM to Continuous Actions Generation.

Thus, for continuous tasks learning, the next action prediction is written as:

$$\mathbf{A}_{k+1} = \mathbf{\Phi}(\mathbf{O}_k, \mathbf{S}_k). \tag{25}$$

As described in Sections III-C to III-E, GPA-RAM can be effectively applied to discrete tasks. To extend this general framework to continuous tasks, we adapt GPA and RAM within the ACT framework through two key modifications (Fig. 4). First, we replace the Transformer encoders with a single-stage RAM, removing the coarse-to-fine structure used in the discrete action benchmark. Different from Equation (14), the updated feature extraction process is formulated as:

$$\widetilde{\mathbf{F}}_{O} = \operatorname{Conv}(\mathbf{O}_{k}),$$

$$\widetilde{\mathbf{F}}_{RAM} = \widetilde{\phi}_{RAM} \left(\widetilde{\mathbf{F}}_{O}, \operatorname{MLP}(\mathbf{S}_{k}) \right).$$
(26)

Second, we integrate a ResNet-based GPA module with the RAM. Specifically, the GPA module fuses grasp features with RAM features, as Equation (15):

$$\widetilde{\mathbf{F}}_{GPA} = \widetilde{\phi}_{GPA} \left(\mathbf{O}_k, \widetilde{\mathbf{F}}_{RAM} \right). \tag{27}$$

Subsequently, a Transformer decoder is employed to generate continuous action outputs based on the fused features:

$$\mathbf{A}_{k+1}^{'} = \text{TransformerDecoder}(\widetilde{\mathbf{F}}_{GPA}, \mathbf{E}),$$
 (28)

where **E** denotes the positional embeddings utilized as the decoder's query. The total loss for continuous tasks is then computed by comparing the predicted actions with the ground-truth actions:

$$\mathcal{L}_{ALOHA} = \left\| \mathbf{A}_{k+1}^{'} - \mathbf{A}_{k+1} \right\|_{2}^{2}, \tag{29}$$

where A_{k+1} denotes the ground-truth continuous action. The model is trained end-to-end by minimizing the loss:

$$\widetilde{\boldsymbol{\theta}}^* = \arg\min_{\boldsymbol{\theta}} \mathcal{L}_{ALOHA},\tag{30}$$

where θ represents the parameters of the entire network.

IV. SIMULATION AND EXPERIMENTAL VERIFICATIONS

To demonstrate the superiority of the proposed GPA-RAM over other methods, we conducted comprehensive experiments across various platforms (CoppeliaSim, MuJoCo, and real-world environments). The evaluation involved diverse robotic systems, including the Franka Emika Panda and ALOHA dual-arm robot in simulation, as well as the UR5 manipulator and ARX R5 dual-arm system in the real world. These experiments

TABLE I

MULTI-TASK PERFORMANCE EVALUATION ON RLBENCH. THE TABLE SUMMARIZES THE SUCCESS RATES ACROSS 18 MANIPULATION TASKS. GPA-RAM
ACHIEVES A NEW SOTA AVERAGE SUCCESS RATE OF 87.5%, OUTPERFORMING PREVIOUS BASELINES SUCH AS RVT2 AND ARP⁺. RAM ALSO
DEMONSTRATES ROBUST PERFORMANCE WITH AN 84.7% SUCCESS RATE, OUTPERFORMING ARP (81.6%) BY A MARGIN OF 3.1%.

Model	Avg. Success ↑	Avg. Rank ↓	Close Jar	Drag Stick	Insert Peg	Meat off Grill	Open Drawer	Place Cups	Place Wine	Push Buttons
Image-BC (CNN) [35]	1.3	12.14	0	0	0	0	4	0	0	0
Image-BC (ViT) [35]	1.3	12.31	0	0	0	0	0	0	0	0
C2F-ARM-BC [43]	20.1	11.08	24	24	4	20	20	0	8	72
HiveFormer [44]	45.3	9.25	52.0	76.0	0.0	100.0	52.0	0.0	80	84
Peract [12]	49.4	7.94	55.2 ± 4.7	89.6 ± 4.1	5.6 ± 4.1	70.4 ± 2.0	88.0 ± 5.7	2.4 ± 3.2	44.8 ± 7.8	92.8 ± 3.0
PolarNet [14]	46.4	8.33	36.0	92.0	4.0	100.0	84.0	0.0	40	96
Act3D [13]	65.0	5.83	92.0	92.0	27.0	94.0	93.0	3.0	80	99
RVT [15]	62.9	6.61	52.0 ± 2.5	99.2 ± 1.6	11.2 ± 3.0	88.0 ± 2.5	71.2 ± 6.9	4.0 ± 2.5	91.0 ± 5.2	92.0 ± 0.0
RVT2 [16]	79.3	4.53	99.0 ± 1.0	98.0 ± 2.0	43.0 ± 7.7	98.0 ± 2.0	78.0 ± 8.3	28.0 ± 7.5	95.0 ± 1.7	96.0 ± 0.0
ARP [17]	81.6	4.19	97.6	88.0	53.2	96.0	90.4	48	92.0	100.0
ARP+ [17]	84.9	3.28	95.2	99.2	78.4	97.6	92.8	48.8	96.0	100.0
RAM (ours)	84.7	3.22	100.0 ± 0.0	100.0 ± 0.0	77.0 ± 1.7	98.0 ± 2.0	78.0 ± 6.6	47.0 ± 3.3	93.0 ± 3.3	96.0 ± 0.0
GPA-RAM (ours)	87.5	2.28	100.0 ± 0.0	100.0 ± 0.0	95.0 ± 1.7	100.0 ± 0.0	84.0 ± 6.7	40.0 ± 4.0	100.0 ± 0.0	89.8 ± 3.2
Model	Put in Cupboard	Put in Drawer	Put in Safe	Screw Bulb	Slide Block	Sort Shape	Stack Blocks	Stack Cups	Sweep to Dustpan	Turn Tap
Image-BC (CNN) [35]	0	8	4	0	0	0	0	0	0	8
Image-BC (ViT) [35]	0	0	0	0	0	0	0	0	0	16
C2F-ARM-BC [43]	0	4	12	8	16	8	0	0	0	68
HiveFormer [44]	32.0	68.0	76.0	8.0	64.0	8.0	8.0	0.0	28.0	80
Peract [12]	28.0 ± 4.4	51.2 ± 4.7	84.0 ± 3.6	17.6 ± 2.0	74.0 ± 13.0	16.8 ± 4.7	26.4 ± 3.2	2.4 ± 2.0	52.0 ± 0.0	88.0 ± 4.4
PolarNet [14]	12.0	32.0	84.0	44.0	56.0	12.0	4.0	8.0	52.0	80
Act3D [13]	51.0	90.0	95.0	47.0	93.0	8.0	12.0	9.0	92.0	94
RVT [15]	49.6 ± 3.2	88.0 ± 5.7	91.2 ± 3.0	48.0 ± 5.7	81.6 ± 5.4	36.0 ± 2.5	28.8 ± 3.9	26.4 ± 8.2	72.0 ± 0.0	93.6 ± 4.1
RVT2 [16]	59.0 ± 4.4	96.0 ± 0.0	96.0 ± 4.0	89.0 ± 3.3	81.0 ± 3.3	47.0 ± 3.3	62.0 ± 6.0	77.0 ± 3.3	98.0 ± 2.0	87.5 ± 3.7
ARP [17]	68.0	99.2	94.4	85.6	98.4	35.2	55.2	76.8	90.4	100.0
ARP+ [17]	69.6	98.4	86.4	89.6	92.8	46.4	63.2	80.0	97.6	96.0
RAM (ours)	79.0 \pm 4.4	100.0 ± 0.0	96.0 ± 2.8	88.0 ± 0.0	91.0 ± 1.7	55.0 ± 5.2	70.4 \pm 5.4	62.0 ± 6.6	100.0 ± 0.0	94.0 ± 3.5
GPA-RAM (ours)	70.0 ± 2.0	100.0 ± 0.0	98.0 \pm 2.0	92.0 \pm 0.0	93.0 ± 1.7	66.0 \pm 2.0	65.6 ± 2.0	84.8 ± 1.6	100.0 ± 0.0	97.0 ± 3.3

covered a wide range of settings, spanning from discrete tasks (e.g., RLBench) to continuous manipulation tasks in both simulated and physical scenarios.

A. Benchmarks in Simulation

In simulation, this paper evaluated the proposed method using the RLBench [11] and ALOHA [9] benchmarks. The RLBench benchmark, simulated on CoppeliaSim [45] platform, includes 18 tasks, where existing methods frequently encounter difficulties in high-precision grasping and placement tasks, such as inserting a ring onto a square peg, and placing a triangular prism into a shape sorter. Each demonstration consists of RGB-D images from the front, left shoulder, right shoulder, and wrist camera views, a language description, and the states of the Franka Panda robot at each time step. Keyframe discovery, selecting critical task frames (e.g., zero velocity or gripper state change), is exploited to reduce data redundancy and improve model learning efficiency following [12], [13], [15], [16]. The ALOHA benchmark, generated on MuJoCo [46] platform, contains two fine-grained bimanual tasks: a cube transfer task and an insertion task. Each demonstration provides RGB images from multiview cameras and the states of the ALOHA dual-arm robot at each time step.

B. Baselines

For RLBench, the proposed GPA-RAM was compared with leading methods, including those tailored directly for 3D visual observations such as 3D point clouds and voxel grids (C2F-ARM-BC [12], [43], Peract [12], PolarNet [14], and Act3D [13]), and the latest image-based approaches (Image-BC (CNN) [12], [35], Image-BC (ViT) [12], [35], HiveFormer

[44], RVT [15], RVT2 [16]) and ARP⁺ [17]. They are all based on Transformer or CNN. The proposed method is a Mamba-based method introduced in this multi-task benchmark. For ALOHA dataset, we adapted the proposed RAM and GPA into Action Chunking with Transformers [9] (abbreviated as ACT, and different from Act3D), and compared them against the top-performing methods, i.e., BC-ConvMLP [35], BeT [47], RT-1 [38], VINN [48], and ACT [9].

C. Implementation Details

The proposed GPA-RAM and the most competitive baseline are trained and tested on three RTX 4090 GPUs for the RL-Bench tasks. The training is conducted with a batch size of 24 over 99 epochs, starting with a learning rate of 0.0018, which is dynamically adjusted using the Cosine Annealing Learning Rate scheduler. Each task is trained on 100 demonstrations and tested four times on 25 unseen scenarios, using models from the final 30 training epochs. The best-performing model is selected for the final success rate comparison. For the ALOHA tasks, training is performed on a single RTX 4090 GPU. Each task is trained with 50 scripted demonstrations, and the best model during training is chosen for testing. Each task is tested with 50 different trials. Since the ALOHA dataset lacks language features, the language components in GPA-RAM are replaced with the features of the current robot arm state. In our implementation, we employ M2T2 [49] as the grasp pose detector for RLBench tasks, which are trained in a multi-task manner. Conversely, for ALOHA tasks, we use ResNet [50] and a single-task training approach. We do not consider inference time for RLBench, as it is a discrete action generation benchmark.

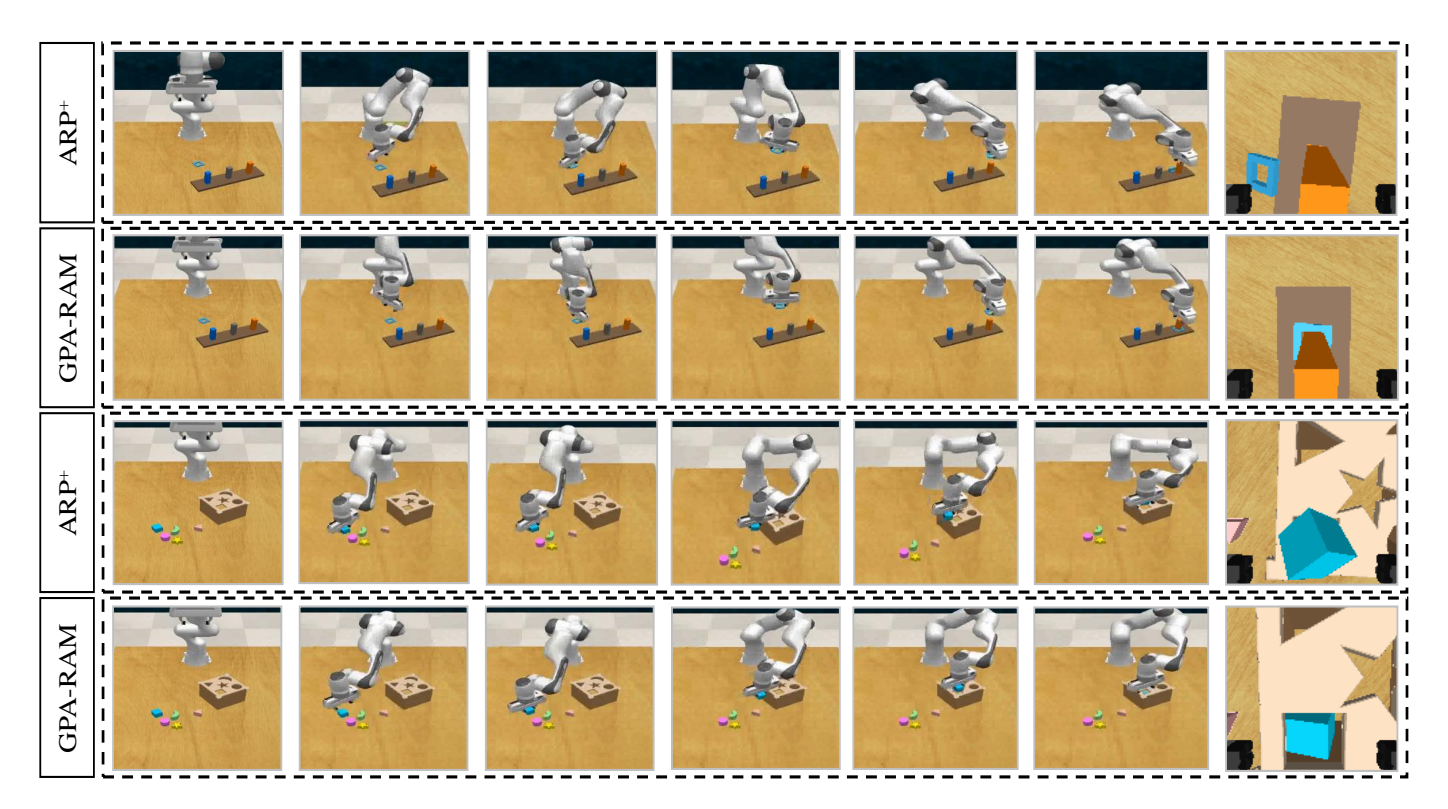


Fig. 5. Qualitative Comparison of the previous SOTA (ARP⁺) and our GPA-RAM on RLBench Tasks. In the first row, ARP⁺ fails in the "Insert the square ring onto the orange peg" task due to an inaccurate initial grasping pose and insufficient pose adjustment. In the third row, it fails in the "Sort the cyan cube into the cube slot of the shape sorter" task because of the erroneous initial grasping pose.

D. Evaluation Metrics

To rigorously evaluate our models against prior work, we report performance across 18 tasks from the RLBench benchmark. We employ two key metrics to measure performance:

- Average Success Rate (%): This is the primary metric for overall performance. It is calculated as the mean percentage of successful episodes across 18 tasks. A higher value indicates better overall task-solving capability.
- Average Rank (Avg. Rank): To assess the consistency and comprehensive performance of each model across the full task suite, we also compute the Average Rank. For each task, all models are ranked based on their success rate (e.g., 1st, 2nd, 3rd...). We then average these ranks across all 18 tasks for each model. A lower Average Rank signifies a more robust and consistently high-performing model across the entire benchmark.

E. Results of RLBench-18 Tasks

Table I summarizes the evaluation results across 18 RL-Bench tasks. In this multi-task imitation learning, the proposed GPA-RAM achieves SOTA performance in terms of both average success rate and task consistency. For the average success rate, our GPA-RAM (87.5%) surpasses the previous SOTA method, ARP⁺ [17] (84.9%). The improvement is even more pronounced when compared to the widely-used RVT2 [16] baseline, where our method shows an 8.2% increase (from 79.3%). This SOTA performance is reinforced by the Average Rank metric (lower is better), where our GPA-RAM (2.28) also achieves the top score, demonstrating superior consistency

compared to ARP⁺ (3.28) and RVT2 (4.53). Notably, the standalone RAM achieves an 84.7% success rate and an Average Rank of 3.22. This performance is comparable to the previous SOTA ARP⁺, and superior in terms of ranking, while outperforming the RVT2 baseline by 5.4%, thereby validating the effective spatial feature extraction capability of RAM.

This advantage in precision is also evident when comparing GPA-RAM (95.0%) directly against ARP⁺ (78.4%) in the "Insert Peg" task. The "Grasp-Pretraining Augmentation" (GPA) component provides a clear benefit in other tasks demanding high-precision grasping. For example, in "Stack Cups", our method achieves 84.8% success compared to ARP⁺'s 80.0%. Furthermore, in the challenging "Sort Shape" task, GPA-RAM significantly outperforms ARP⁺ (66.0% vs 46.4%), demonstrating a consistent edge in fine-grained manipulation.

The effectiveness of our GPA module is further validated by comparing GPA-RAM to its non-GPA counterpart, RAM. In the "Stack Cups" and "Sort Shape" tasks, integrating GPA boosts the success rates by **22.8%** (from 62.0% to 84.8%) and **11.0%** (from 55.0% to 66.0%) respectively. This demonstrates that GPA effectively draws on grasping priors learned from pre-trained models to enhance fine-grained manipulation affordance, compensating for the limitations of pure spatial in capturing precise grasping cues.

F. Results of ALOHA Bimanual Tasks

In Table II, a comparison with the most competitive method (ACT [9]) reveals that the proposed GPA-RAM delivered SOTA performance on two ALOHA bimanual tasks in terms of both success rate and inference speed. Each task is divided into

TABLE II
EVALUATION ON ALOHA TASKS. WE REPORT SUCCESS RATES FOR CUBE
TRANSFER AND BIMANUAL INSERTION.

Model	Inference Time	Cube Transfer			
1120401	(fps)	Touch	Lift	Transfer	
BC-ConvMLP [35]	-	34	17	1	
RT-1 [38]	28.7	44	33	2	
VINN [48]	_	13	9	3	
BeT [47]	_	60	51	27	
ACT [9]	61.7	98	86	86	
RAM (ours)	75.2	100	98	98	
GPA-RAM (ours)	71.3	100	100	98	

Model	Inference Time	Bimanual Insertion			
	(fps)	Grasp	Contact	Insert	
BC-ConvMLP [35]	-	5	1	1	
RT-1 [38]	33.3	2	0	1	
VINN [48]	-	6	1	1	
BeT [47]	-	21	4	3	
ACT [9]	61.0	96	92	16	
RAM (ours)	73.0	96	94	32	
GPA-RAM (ours)	70.9	96	94	56	

three subtasks in line with the order of manipulation, and the success rate of the last subtask is equivalent to the overall task success rate. The overall success rate of the cube transferring task increased by 12%, while the bimanual insertion task saw a remarkable improvement of 40%. These demonstrated their effectiveness in planning bimanual cooperation and mastering fine-grained manipulation skills.

In addition to success rates, we explicitly evaluated the inference efficiency. As shown in Table II, our proposed GPA-RAM achieves an inference speed of approximately 71 FPS, which surpasses the strong baseline ACT (~61 FPS) and is significantly faster than RT-1 (~30 FPS). This high throughput is particularly advantageous for processing continuous visual streams in dynamic environments. Unlike pure Transformer architectures where latency spikes with increased spatial token density, RAM maintains superior efficiency, ensuring the system's responsiveness to rapid visual changes. This indicates that incorporating the grasp pretraining module enhances robustness without compromising real-time control capabilities.

Meanwhile, the proposed RAM and GPA-RAM excel in other subtasks, including touching, lifting, grasping, and making contact. Fig. 6 provides a more qualitative comparison of GPA-RAM and the previous SOTA (ACT). Furthermore, M2T2 [49] and ResNet [50] were employed as grasp pose detectors for RLBench and ALOHA datasets, respectively. Since both GPAs apply in RLBench and ALOHA delivered notable boosts for manipulation, this demonstrates that our proposed GPA framework is generic and robust to different architectures of pretrained grasp pose detectors.

G. Real-world Experiments

Experimental Setup. In real-world experiments, the hardware setup was demonstrated in Fig. 7. For discrete action generation, we utilized a 6-DOF UR5 manipulator with a Robust Motion GB-17-60 gripper. The vision system, adapted from

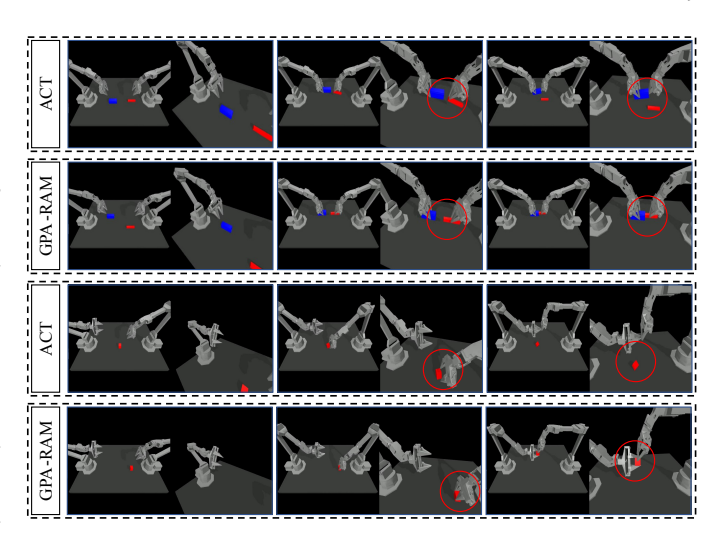


Fig. 6. Qualitative Comparison of the Proposed GPA-RAM and the Previous SOTA method (ACT) on ALOHA Bimanual Tasks. The top two rows illustrate the bimanual insertion task, where ACT struggles due to suboptimal grasping and unachievable in-hand pose adjustment of 2-finger grippers, leading to insertion failures. The bottom two rows depict the cube transfer task, where ACT fails to grasp the target cube. In contrast, GPA-RAM completes both tasks successfully, demonstrating evident advantages in execution.

TABLE III
DISCRETE ACTION TASKS PERFORMANCE ON REAL-WORLD.

Task	RVT2	ARP^+	GPA-RAM
Place cylindrical block in drawer	70%	90%	100%
Place quadrangular block in drawer	70%	80%	90%
Place hexagonal block in drawer	80%	90%	100%
Put bottle on middle shelf	60%	80%	90%
Put bottle on top shelf	60%	80%	80%
Grasp and insert round hole in peg	50%	50%	70%
Grasp and insert square hole in peg	30%	40%	50%

the RLBench four-camera layout, employed two RealSense D455 cameras (frontal and overhead) as shown in Fig. 7, with data collected via a custom joystick interface. For continuous action generation, a dual-arm ARX R5 system was employed. This setup featured three RealSense D405 cameras (mounted on the head and both wrists), with data acquisition facilitated through direct teleoperation.

Real-world Tasks. As shown in Fig. 8, Table III and IV, real-robot experiments involved seven discrete tasks—including block-to-drawer placement (cylindrical, hexagonal, quadrangular), bottle-to-shelf arrangement (middle and top shelves), and tight-tolerance insertion (round and square peg-in-hole)—where object poses varied significantly between training and testing. Additionally, three continuous tasks (plate transferring, tabletop organization, and bowl stacking) were deployed on the ARX R5 dual-arm robot. For more examples, see the supplementary materials.

The training dataset comprised 20 demonstrations for each discrete task and 50 demonstrations for each continuous task. Each task was tested in 10 unseen scenarios. By leveraging learning from demonstrations, our method aims to generate collision-free trajectories capable of handling high-precision manipulation constraints.

Real-world Experimental Results. The real-world experimental results in Table III demonstrate the superiority of GPA-RAM in efficiently learning diverse manipulation tasks with

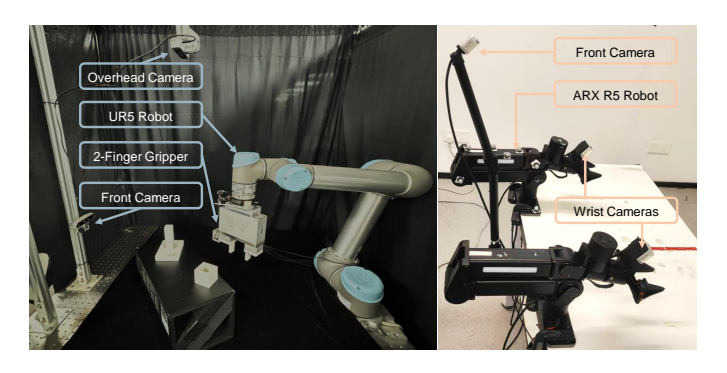


Fig. 7. Real-world experimental setups for discrete action generation (left) and continuous action generation (right).

TABLE IV CONTINUOUS ACTION TASKS PERFORMANCE ON REAL-WORLD.

Task	ACT	RAM	GPA-RAM
Plate transferring	80%	90%	100%
Tabletop Organization	70%	80%	90%
Bowl Stacking	60%	80%	90%

few demonstrations. Our method consistently outperforms both the baseline RVT2 and the competitor ARP⁺.

In discrete tasks, GPA-RAM excelled in placing blocks of varying shapes, achieving near-perfect success rates (90%-100%) and demonstrating remarkable grasping adaptability. For spatial tasks like placing bottles on shelves, the method showcased its ability to plan collision-free paths in constrained environments. Although peg-in-hole tasks posed challenges due to stringent alignment requirements, GPA-RAM still achieved respectable success rates (70% and 50%), surpassing baselines by effectively handling contact-rich insertions.

In the introduced continuous action tasks, GPA-RAM exhibited exceptional temporal consistency and bimanual coordination. It achieved a 100% success rate in plate transferring, significantly outperforming ACT (80%) and RAM (90%). In complex, long-horizon tasks such as tabletop organization and bowl stacking, our method maintained a high success rate of 90%, proving its robustness in handling dynamic object interactions where baselines often failed to maintain stability.

V. ABLATION STUDY

We conducted ablation studies of our proposed GPA-RAM in 18 RLBench tasks and 2 ALOHA bimanual cooperation tasks to investigate the effect of its key design choices.

A. Ablations on RLBench-18 Tasks

GPA-RAM set a new SOTA with an average success rate of 87.5% across the 18 tasks in RLbench and the ablation results are presented in Table V. All ablations are trained in multi-task settings, consistent with GPA-RAM.

RAM. This variant excludes the GPA module from GPA-RAM, achieving an average success rate of 84.7% across the 18 tasks in RLBench. While this exceeds RVT2 [16] by 5.4%, the method without GPA falls short by 2.8% compared to the proposed GPA-RAM.



Fig. 8. Examples of GPA-RAM in the real world. Top row: Grasp and insert the square hole into the square peg. Second row: Grasp and place the cylindrical block in the drawer. Third row: Stack bowl. Bottom row: Transfer the plate.

TABLE V ABLATIONS OF GPA-RAM ON RLBENCH-18 TASKS.

Model	Avg. Success	Difference
GPA-RAM	87.5%	_
RAM	84.7%	-2.8%
C-RAM	66.6%	-20.9%
GPA-C-RAM	69.3%	-18.2%
GPA-RVT2	84.2%	-3.3%

C-RAM. This configuration removes the fine stage (F-RAM) from the RAM and deploys only the single-stage RAM, achieving a success rate of 66.6% on RLbench.

GPA-C-RAM. The GPA module is integrated into the C-RAM module. Compared to C-RAM, this improved version achieves a 2.7% improvement on the average success rate.

GPA-RVT2. By integrating RVT2 with the proposed general-purpose GPA framework, the task success rate improves by 4.9% over original RVT2. Nevertheless, GPA-RVT2 still underperforms our proposed GPA-RAM model by 3.3%.

B. Ablations on ALOHA Bimanual Tasks

The proposed GPA-RAM is adapted into the ACT method, and achieving the best performance with success rates of 98% and 56% on the cube transferring and bimanual insertion tasks, respectively, at a control frequency of 50 Hz. Additionally, we conduct experiments at 100 Hz to further evaluate the model's performance under high-frequency servoing. The ablations were trained in single-task settings, summarized in Table VI.

RAM. By removing the GPA module, the success rate for the cube transferring task stays the same as GPA-RAM, but it declines by 24% for the bimanual insertion task. Besides,

TABLE VI ABLATIONS OF GPA-RAM ON ALOHA TASKS.

Frequency	Model	Avg.	Success	Difference		
		Transfer	Insertion	Transfer	Insertion	
50Hz	GPA-RAM	98%	56%	-	-	
	RAM	98%	32%	-0%	-24%	
	GPA-ACT	98%	38%	-0%	-18%	
100Hz	GPA-RAM	90%	40%	-	-	
	RAM	88%	30%	-2%	-10%	
	GPA-ACT	86%	30%	-4%	-10%	

it still outperforms ACT by 12% and 16% on the transferring and insertion tasks, respectively.

GPA-ACT. This model integrates ACT with the proposed GPA framework, achieving 12% and 22% higher success rates than the original ACT on the two ALOHA tasks, respectively. However, it exhibits an 18% performance drop in the Insertion task relative to the proposed GPA-RAM.

The cube transferring task is relatively easy such that all the ablations are competent for this task. Moreover, the proposed GPA-RAM likewise demonstrates its advantages under higher-frequency task settings (100 Hz). Despite a slight drop in success rates, it still outperforms other methods.

To conclude, the adoption of the proposed RAM and GPA can improve the success rate of diverse robotic manipulation tasks, including high-precision discrete manipulation and bimanual continuous coordination. The ablation results demonstrated that both the learning framework GPA and the architecture design RAM can enhance the performance of different network architectures and task settings.

VI. CONCLUSIONS AND LIMITATIONS

This paper proposes a novel pipeline, GPA-RAM, which addresses the challenges of fine-grained robotic manipulation by decomposing manipulation tasks into spatial feature extraction and grasping skill learning. First, GPA integrates a pretrained grasp pose detector to enhance fine-grained grasping perception. Notably, it introduces a data-efficient augmentation strategy by explicitly leveraging grasping priors inherent in task demonstrations, eliminating the need for additional annotations. Complementarily, RAM leverages multi-modal attention mechanisms to achieve efficient inference speed and robust spatial perception. By synergizing these two modules, the unified GPA-RAM framework achieves both precise grasping and efficient task execution, mitigating the reliance on complex pose adjustments and collision avoidance. Extensive empirical evaluations verify the effectiveness and generalizability of our method across diverse task settings, robotic systems, and camera configurations. Furthermore, ablation studies highlight the modularity of our approach, demonstrating the complementary roles of GPA and RAM in boosting the performance of various architectures.

While GPA-RAM demonstrates significant performance gains, particularly in tasks requiring high-precision grasping, we also identify a potential limitation and area for future work. Our results indicate that in a few tasks emphasizing placement or pushing flexibility (such as 'Place Cups' or 'Push Buttons'), the GPA-augmented model performed slightly below

its non-GPA counterpart. We hypothesize this may be due to a trade-off: the GPA module's strong focus on optimizing the initial grasp pose might induce a subtle bias toward the grasping phase. This intense focus could, in some scenarios, constrain the model's maneuverability for subsequent manipulation steps. This suggests a potential balance to be struck between grasp-pose pretraining and the adaptability required for downstream planning. Investigating this trade-off and developing methods to dynamically balance these two skills remains a valuable direction for future research.

REFERENCES

- [1] Y. Mei, J. Sun, Z. Peng, F. Deng, G. Wang, and J. Chen, "Rog-sam: A language-driven framework for instance-level robotic grasping detection," *IEEE Transactions on Multimedia*, vol. 27, pp. 3057–3068, 2025.
- [2] Y. Cui, Z. Zou, X. Ye, X. Tan, Z. Li, and Z. Fang, "Coupling and decoupling: Towards temporal feedback for 3d object detection," *IEEE Transactions on Multimedia*, vol. 27, pp. 7230–7242, 2025.
- [3] X. Yin, F. Pan, G. An, Y. Huo, Z. Xie, and S.-E. Yoon, "Openslot: Mixed open-set recognition with object-centric learning," *IEEE Transactions on Multimedia*, vol. 27, pp. 6019–6030, 2025.
- [4] M. Tan, P. Chen, H. Zhi, J. Mai, B. Rosman, D. Ji, and R. Zeng, "Source-free elastic model adaptation for vision-and-language navigation," *IEEE Transactions on Multimedia*, vol. 27, pp. 3953–3965, 2025.
- [5] S. Zhang, Y. Qiao, Q. Wang, L. Guo, Z. Wei, and J. Liu, "Flexvln: Flexible adaptation for diverse vision-and-language navigation tasks," *IEEE Transactions on Multimedia*, vol. 27, pp. 6307–6318, 2025.
- [6] A. Vaswani, N. Shazeer, N. Parmar, J. Uszkoreit, L. Jones, A. N. Gomez, L. Kaiser, and I. Polosukhin, "Attention is all you need," in *Advances in Neural Information Processing Systems*, vol. 30, 2017, p. 6000–6010.
- [7] J. Ho, A. Jain, and P. Abbeel, "Denoising diffusion probabilistic models," Advances in neural information processing systems, vol. 33, pp. 6840–6851, 2020.
- [8] Y. Chen, A. Li, D. Wu, and L. Zhou, "Toward general cross-modal signal reconstruction for robotic teleoperation," *IEEE Transactions on Multimedia*, vol. 26, pp. 3541–3553, 2024.
- [9] T. Z. Zhao, V. Kumar, S. Levine, and C. Finn, "Learning fine-grained bimanual manipulation with low-cost hardware," in *Proceedings of Robotics: Science and Systems (RSS)*, 2023.
- [10] C. Chi, Z. Xu, C. Pan, E. Cousineau, B. Burchfiel, S. Feng, R. Tedrake, and S. Song, "Universal manipulation interface: In-the-wild robot teaching without in-the-wild robots," in *Proceedings of Robotics: Science and Systems (RSS)*, 2024.
- [11] S. James, Z. Ma, D. R. Arrojo, and A. J. Davison, "Rlbench: The robot learning benchmark & learning environment," *IEEE Robotics and Automation Letters*, vol. 5, no. 2, pp. 3019–3026, 2020.
- [12] M. Shridhar, L. Manuelli, and D. Fox, "Perceiver-actor: A multi-task transformer for robotic manipulation," in *Proceedings of the Conference* on Robot Learning (CoRL), vol. 205, 2022, pp. 785–799.
- [13] T. Gervet, Z. Xian, N. Gkanatsios, and K. Fragkiadaki, "Act3D: 3D feature field transformers for multi-task robotic manipulation," in 7th Annual Conference on Robot Learning, 2023.
- [14] S. Chen, R. Garcia, C. Schmid, and I. Laptev, "Polarnet: 3d point clouds for language-guided robotic manipulation," in *In 7th Annual Conference* on Robot Learning (CoRL), 2023.
- [15] A. Goyal, J. Xu, Y. Guo, V. Blukis, Y.-W. Chao, and D. Fox, "Rvt: Robotic view transformer for 3D object manipulation," in *Proceedings* of the Conference on Robot Learning (CoRL). PMLR, 2023.
- [16] A. Goyal, V. Blukis, J. Xu, Y. Guo, Y.-W. Chao, and D. Fox, "Rvt2: Learning precise manipulation from few demonstrations," in *Robotics: Science and Systems*, 2024.
- [17] X. Zhang, Y. Liu, H. Chang, L. Schramm, and A. Boularias, "Autoregressive action sequence learning for robotic manipulation," *IEEE Robotics and Automation Letters*, vol. 10, no. 5, pp. 4898–4905, 2025.
- [18] C. Li, J. Yang, P. Zhang, M. Gao, B. Xiao, X. Dai, L. Yuan, and J. Gao, "Efficient self-supervised vision transformers for representation learning," in *The International Conference on Learning Representations* (ICLR), 2022.
- [19] A. Gu, K. Goel, and C. Ré, "Efficiently modeling long sequences with structured state spaces," 2022. [Online]. Available: https://arxiv.org/abs/2111.00396

[20] A. Gu and T. Dao, "Mamba: Linear-time sequence modeling with selective state spaces," in Conference on Language Modeling, 2024.

- [21] X. Zhong, T. Gong, J. Yu, C. Zhou, X. Zhong, and Q. Liu, "Rignet: Robot intention grasp for dense stacked targets with multi-task siamese schema through rois learning," *IEEE Transactions on Automation Sci*ence and Engineering, vol. 22, pp. 10354–10367, 2025.
- [22] C. Tang, D. Huang, W. Dong, R. Xu, and H. Zhang, "Foundationgrasp: Generalizable task-oriented grasping with foundation models," *IEEE Transactions on Automation Science and Engineering*, vol. 22, pp. 12418–12435, 2025.
- [23] P. Xu, H. Cheng, J. Wang, and M. Q.-H. Meng, "Learning to reorient objects with stable placements afforded by extrinsic supports," *IEEE Transactions on Automation Science and Engineering*, vol. 21, no. 4, pp. 5653–5664, 2024.
- [24] S. Yang, W. Zhang, R. Song, J. Cheng, H. Wang, and Y. Li, "Watch and act: Learning robotic manipulation from visual demonstration," *IEEE Transactions on Systems, Man, and Cybernetics: Systems*, vol. 53, no. 7, pp. 4404–4416, 2023.
- [25] J. Zhao, Z. Wang, L. Zhao, and H. Liu, "A learning-based two-stage method for submillimeter insertion tasks with only visual inputs," *IEEE Transactions on Industrial Electronics*, vol. 71, no. 7, pp. 7381–7390, 2024.
- [26] K. Xu, Z. Zhou, J. Wu, H. Lu, R. Xiong, and Y. Wang, "Grasp, see, and place: Efficient unknown object rearrangement with policy structure prior," *IEEE Transactions on Robotics*, vol. 41, pp. 464–483, 2025.
- [27] C. Chi, S. Feng, Y. Du, Z. Xu, E. Cousineau, B. Burchfiel, and S. Song, "Diffusion policy: Visuomotor policy learning via action diffusion," in Proceedings of Robotics: Science and Systems, 2023.
- [28] K. Black, M. Nakamoto, P. Atreya, H. R. Walke, C. Finn, A. Kumar, and S. Levine, "Zero-shot robotic manipulation with pre-trained image-editing diffusion models," in *The International Conference on Learning Representations (ICLR)*, 2024.
- [29] H. Wu, Y. Jing, C. Cheang, G. Chen, J. Xu, X. Li, M. Liu, H. Li, and T. Kong, "Unleashing large-scale video generative pre-training for visual robot manipulation," in *The International Conference on Learning Representations (ICLR)*, 2024.
- [30] P. Li, H. Wu, Y. Huang, C. Cheang, L. Wang, and T. Kong, "Gr-mg: Leveraging partially-annotated data via multi-modal goal-conditioned policy," *IEEE Robotics and Automation Letters*, 2025.
- [31] C. Wen, X. Lin, J. So, K. Chen, Q. Dou, Y. Gao, and P. Abbeel, "Any-point trajectory modeling for policy learning," arXiv preprint arXiv:2401.00025, 2023.
- [32] X. Li, B. He, Z. Wang, Y. Zhou, G. Li, and X. Li, "Toward cognitive digital twin system of human-robot collaboration manipulation," *IEEE Transactions on Automation Science and Engineering*, vol. 22, pp. 6677–6690, 2025.
- [33] H. Bharadhwaj, A. Gupta, V. Kumar, and S. Tulsiani, "Towards generalizable zero-shot manipulation via translating human interaction plans," in 2024 IEEE International Conference on Robotics and Automation (ICRA), 2024, pp. 6904–6911.
- [34] Z. Jia, B. Qingwen, W. Bangjun, X. Wenke, C. Li, D. Hao, S. Haoming, W. Dong, H. Di, L. Ping, C. Heming, Z. Bin, L. Xuelong, Q. Yu, and L. Hongyang, "Learning manipulation by predicting interaction," in *Proceedings of Robotics: Science and Systems (RSS)*, 2024.
- [35] E. Jang, A. Irpan, M. Khansari, D. Kappler, F. Ebert, C. Lynch, S. Levine, and C. Finn, "Bc-z: Zero-shot task generalization with robotic imitation learning," in *Proceedings of the 5th Conference on Robot Learning*, ser. Proceedings of Machine Learning Research, A. Faust, D. Hsu, and G. Neumann, Eds., vol. 164. PMLR, 08–11 Nov 2022, pp. 991–1002.
- [36] O. Mees, L. Hermann, and W. Burgard, "What matters in language conditioned robotic imitation learning over unstructured data," *IEEE Robotics and Automation Letters*, vol. 7, no. 4, pp. 11 205–11 212, 2022.
- [37] T. Ma, J. Zhou, Z. Wang, R. Qiu, and J. Liang, "Contrastive imitation learning for language-guided multi-task robotic manipulation," in 8th Annual Conference on Robot Learning (CoRL), 2024.
- [38] A. Brohan, N. Brown, J. Carbajal, and et al., "Rt-1: Robotics transformer for real-world control at scale," in *Proceedings of Robotics: Science and Systems (RSS)*, 2022.
- [39] —, "Rt-2: Vision-language-action models transfer web knowledge to robotic control," arXiv preprint arXiv:2307.15818, 2023.
- [40] Y. Liu, S. Liu, B. Chen, Z.-X. Yang, and S. Xu, "Fusion-perception-to-action transformer: Enhancing robotic manipulation with 3-d visual fusion attention and proprioception," *IEEE Transactions on Robotics*, vol. 41, pp. 1553–1567, 2025.

[41] A. Gu, K. Goel, and C. Ré, "Efficiently modeling long sequences with structured state spaces," in *The International Conference on Learning Representations (ICLR)*, 2022.

- [42] A. Radford, J. W. Kim, C. Hallacy, A. Ramesh, G. Goh, S. Agarwal, G. Sastry, A. Askell, P. Mishkin, J. Clark et al., "Learning transferable visual models from natural language supervision," in *International Conference on Machine Learning (ICML)*, 2021, pp. 8748–8763.
- [43] S. James, K. Wada, T. Laidlow, and A. J. Davison, "Coarse-to-fine q-attention: Efficient learning for visual robotic manipulation via discretisation," in *Proceedings of the IEEE/CVF Conference on Computer Vision and Pattern Recognition (CVPR)*, 2022, pp. 13739–13748.
- [44] P.-L. Guhur, S. Chen, R. G. Pinel, M. Tapaswi, I. Laptev, and C. Schmid, "Instruction-driven history-aware policies for robotic manipulations," in Proceedings of the Conference on Robot Learning (CoRL). PMLR, 2023, pp. 175–187.
- [45] E. Rohmer, S. P. N. Singh, and M. Freese, "V-rep: A versatile and scalable robot simulation framework," in 2013 IEEE/RSJ International Conference on Intelligent Robots and Systems, 2013, pp. 1321–1326.
- [46] E. Todorov, T. Erez, and Y. Tassa, "Mujoco: A physics engine for model-based control," in 2012 IEEE/RSJ International Conference on Intelligent Robots and Systems. IEEE, 2012, pp. 5026–5033.
- [47] N. M. Shafiullah, Z. Cui, A. A. Altanzaya, and L. Pinto, "Behavior transformers: Cloning k modes with one stone," in *Advances in Neural Information Processing Systems*, S. Koyejo, S. Mohamed, A. Agarwal, D. Belgrave, K. Cho, and A. Oh, Eds., vol. 35. Curran Associates, Inc., 2022, pp. 22955–22968.
- [48] J. Pari, N. M. Shafiullah, S. P. Arunachalam, and L. Pinto, "The surprising effectiveness of representation learning for visual imitation," arXiv preprint arXiv:2112.01511, 2021.
- [49] W. Yuan, A. Murali, A. Mousavian, and D. Fox, "M2t2: Multi-task masked transformer for object-centric pick and place," in *Conference* on Robot Learning, vol. 229, 2023, pp. 3619–3630.
- [50] K. He, X. Zhang, S. Ren, and J. Sun, "Deep residual learning for image recognition," in *Proceedings of the IEEE/CVF Conference on Computer Vision and Pattern Recognition (CVPR)*, 2016, pp. 770–778.